# Numerical Simulation of the Evolution of Solidification Microstructure in Laser Deposition

Zhiqiang Fan[1], Todd E. Sparks[1], Frank Liou[1], Anand Jambunathan[2], Yaxin Bao[1], Jianzhong Ruan[1] and Joseph W. Newkirk[2]

[1]Department of Mechanical and Aerospace Engineering, University Of Missouri–Rolla

[2]Department of Metallurgical Engineering, University Of Missouri–Rolla

1870 Miner Circle, Rolla, MO 65409

Reviewed, accepted August 21, 2007

**Abstract**

A predictive model is developed to simulate the evolution of the solidification microstructure during the laser deposition process. The microstructure model is coupled with a comprehensive macroscopic thermodynamic model. This model simulates dendritic grain structures and morphological evolution in solidification. Based on the cellular automata approach, this microstructure model takes into account the heterogeneous nucleation both within the melt pool and at the substrate/melt interface, the growth kinetics, and preferential growth directions of dendrites. Both diffusion and convection effects are included. This model enables prediction and visualization of grain structures during and after the deposition process. This model is applied to Ti-6Al-4V.

## 1. **Instruction**

Laser deposition is an extension of the laser cladding process. This laser additive manufacturing technique allows quick fabrication of fully-dense metallic components directly from Computer Aided Design (CAD) solid models. The applications of laser deposition include rapid prototyping, rapid tooling and part refurbishment. As shown in Fig. 1, laser deposition uses a focused laser beam as a heat source to create a melt pool on an underlying substrate. Powder material is then injected into the melt pool through nozzles. The incoming powder is metallurgically bonded with the substrate upon solidification. The part is fabricated in a layer by layer manner in a shape that is dictated by the CAD solid model.

The key to the mechanical strength of materials in the as-deposited condition is the microstructure. This study is to model and simulate the evolution of the solidification microstructures during the laser deposition process. In particular, the grain structure of the deposit (new layers) and the heat affected zone (HAZ) is the subject of this paper. The effect of flow velocity and macrosegregation on the formation of microstructure is considered. Cellular automaton (CA) method is adopted to investigate the microstructure evolution. The CA algorithm describes the discrete spatial and temporal evolution of complex systems by applying local (or sometimes long-range) deterministic or probabilistic transformation rules to the cells of a regular (or nonregular) lattice [1]. Compared with other microstructure models, such as Monte Carlo models, front-tracking models, and phase field models, the strength of cellular automaton is such that it combines the computational simplicity and scalability with the physical stringency.

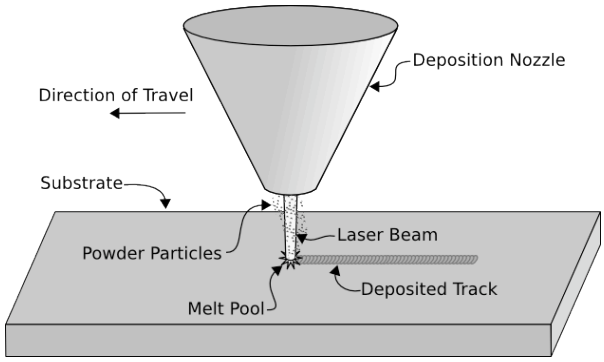


Fig. 1. Schematic of a typical laser deposition system

In this work the evolution of solidification microstructure is simulated on the basis of the physically based probabilistic cellular automaton method developed by Guillemot et al. [2]. The method ensures that: (a) the simulation results are not affected by the type of calculation cells (cubic or hexagonal) used; (b) the dendrites grow preferentially in ⟨10⟩ directions; (c) the kinetics of dendrite-tip growth (primarily the effects of local undercooling, fluid flow and solute concentration) is properly taken into account.

## 2. Mathematical Model

### 2.1 Microscopic Model

The microscopic model is used to simulated heterogeneous nucleation, dendrite growth and grain transport, etc during the laser deposition process. The model is almost identical to the one developed by Guillemot et al. [2] and hence some details of the model will be omitted.

#### 2.1.1 Nucleation

The nucleation algorithm is based on an instantaneous nucleation law, that is, regardless of cooling rate, nucleation occurs as soon as the undercooling reaches a critical value. A Gaussian distribution is used to characterize grain density as a function of undercooling:

$$n(\Delta T) = \int_0^{\Delta T} \frac{dn}{dT'} d\Delta T' = \int_0^{\Delta T} \frac{n_{\max}}{\Delta T_\sigma \sqrt{2\pi}} \exp\left[ -\frac{1}{2} \left( \frac{\Delta T' - \Delta T_N}{\Delta T_\sigma} \right) \right] d\Delta T' \qquad (1)$$

where $\Delta T_N$ is the mean undercooling, corresponding to the maximum of the undercooling distribution, $\Delta T_\sigma$ is the standard deviation, and $n_{max}$ is the maximum density of nucleation sites (grains), given by the integral of total distribution (from zero undercooling to infinite undercooling). These three standard nucleation parameters must be determined experimentally for each melt by measuring the grain density and the corresponding maximum undercooling at recalescence under various cooling conditions [3]. Different nucleation laws are used for the bulk liquid and the substrate/melt-pool interface. Stereological relationships are used for 3D-2D conversion of maximum densities.

Nucleation sites are randomly distributed among the CA cells. For a nucleation site, a critical nucleation undercooling is assigned randomly according to the prescribed Gaussian

distribution, and a crystallographic orientation is also randomly chosen among the predefined classes.

2.1.2 Growth

The dendrite tip velocity is calculated by the following set of equations. Neglecting the kinetic and thermal undercooling, the total dendrite tip undercooling, ΔT, is thesum of a chemical undercooling and a curvature undercooling:

$$\Delta T = mC^l(1-\frac{1}{1-(1-k_p)\Omega_c}) + \frac{2\Gamma}{r} \quad (2)$$

where Γ is the Gibbs-Thomson coefficient (the ratio of solid/liquid interface energy to the melting entropy), $k_p$ is the solute partition coefficient (the ratio of solute concentration in solid to that in liquid) at the solid/liquid interface, $m$ is the liquidus slope, D is the solute diffusion coeffcient in the liquid, $C^l$ is the solute concentration in the bulk liquid far from the dendrite tip.

In Eq. 2, $m$, $k_p$, $D$, and Γ are all temperature dependent, and in addition, $k_p$ depends on the solidification front velocity, V, according to the relationship given by [4]:

$$k_p = \frac{k_0 + a_0 V/D}{1 + a_0 V/D} \quad (3)$$

where $k_0$ is the equilibrium partition ratio, $a_0$ is the length scale related to the interatomic distance and is estimated to be between 0.5 and 5 nm. Assuming equilibrium at the dendrite tip solid/liquid interface, the supersaturation, $\Omega_c$, is defined by:

$$\Omega_c = \frac{C^{s/l} - C}{C^{s/l}(1-k_p)} \quad (4)$$

where $C^{s/l}$ is the solute concentration of the liquid at the solid/liquid interface. $C^{s/l}$ is calculated with the phase diagram of the binary alloy accounting for the curvature effect:

$$T = T_m + mC^{s/l} - \frac{2\Gamma}{r} \quad (5)$$

The dendrite tip velocity, $V_p$ and the radius of curvature at the dendrite tip, r, are linked by using the marginal stability criterion [5]:

$$\sigma^* = \frac{D^l}{V_p r^2}\frac{\Gamma}{mC^{s/l}(1-k_p)} \quad (6)$$

where $D^l$ is the diffusion coefficient of the solute element in the liquid, and σ* the marginal stability constant taken as $1/(4\pi^2)$ [5,6].

The supersaturation, $\Omega_c$, is calculated according to the boundary layer correlation [7]:

$$\Omega_c = Pe_{V_p} \exp(Pe_{V_p}) \left[ E_1(Pe_{V_p}) - E_1(Pe_{V_p}(1 + \frac{4}{A \operatorname{Re}^B Sc^C \sin(\phi/2)})) \right] \tag{7}$$

$$Pe_{V_p} = \frac{rV_p}{2D^l} \tag{7a}$$

$$Pe_V = \frac{rV}{2D^l} \tag{7b}$$

$$Sc = \frac{\mu}{\rho^l D^l} \tag{7c}$$

$$\operatorname{Re} = \frac{4Pe_{V^l}}{Sc} \tag{7d}$$

where $Pe_{V_p}$, $Pe_V$, Sc, Re are the growth Peclet number, the flow Peclet number, the Schmidt number and theReynolds number, respectively. The angle ϕ is defined by the primary growth direction of the dendrite tip and the bulk fluid flow velocity, V. For $Pe_{V_p} \in [10^{-4}, 10]$, $Pe_V \in [10^{-2}, 10]$, and Sc ∈ [50, 500], the parameters A, B, C are taken as 0.5773, 0.6596, 0.5249, respectively. $E_1$ is the integral exponential function given by [8]:

$$E_1(Pe) = \int_{Pe}^{\infty} \frac{\exp(-\tau)}{\tau} d\tau \tag{8}$$

Calculations of the velocity and radius of the dendrite tip are implemented by an iterative approach. Details refer to [7].

2.1.3 Grain Transport

Grain transport in the liquid due to liquid flow and sedimentation is considered. A cluster, defined as an assembly of grains contacting each other, is studied. The relative cluster velocity $\vec{V}_{Cr}$ is described by:

$$\vec{V}_{Cr} = \vec{V}_C - \vec{V} = -\left( \frac{2f_C^{sm}(\rho_s - \rho_l)V_e g}{\rho_l A_e C_D} \right)^{1/2} \vec{y} \tag{9}$$

where $\vec{V}_C$ is the cluster velocity, $\vec{V}$ is the fluid flow velocity surrounding the cluster, $V_e$ is the volume of the cluster, $A_e$ is the area projected in the direction of the relative velocity of the cluster, $f_C^{sm}$ is the internal fraction of solid located in the cluster envelope, which is the average of the internal volume fraction of solid located in the cells defining the cluster, and $C_D$ is the drag coefficient, which is calculated using Ahuja's correlation [9]. The grain transport algorithm will not be repeated here.

2.1.4 Cellular Automaton Simulation of the Solidification Process

The microscopic calculation domain is divided into square CA cells. Each cell is assigned a state index, which is zero when the cell is liquid and a positive integer if it is solid. This latter positive number corresponds to a given crystallographic orientation.

If a nucleation cell v is still liquid, and its temperature, $T_v$, interpolated from the macroscopic model falls below the critical nucleation temperature: $T_v < T_m + mC_v - T_v^{nucl}$, the state index of the cell v is updated accordingly. Here $(T_m + mC_v)$ is the local liquidus temperature of the cell v, and $T_v^{nucl}$ is the undercooling prescribed for the cell v.

This newly nucleated grain is assigned a square shape with diagonals corresponding to the preferential directions of the dendrites stems. The initial length of the diagonals is set to zero. The dendritic growth is controlled by the increase in the length of the four half-diagonals. A decentered polygon algorithm [2] is adopted as the growth algorithm. The details of the growth algorithm are omitted here. The center of the growing shape of the newly nucleated grain is located at the center of the nucleation cell. The growing center of a cell which is not a nucleation cell is generally not in the center of this cell. The growing shape of a cell is generally not a regular square since the effect of the fluid flow on the growth kinetics of the four primary growth directions is considered independently.

**2.2 Macroscopic model**

Figure 2 shows a schematic diagram of the calculation domain, including the substrate, melt pool, remelted zone, deposited layer and part of the gas region. The governing equations for the macroscopic model are described in detail in reference [10] and are summarized in Table 1. An important difference between the model used here and that described in reference [10] is that here the species conservation is included.

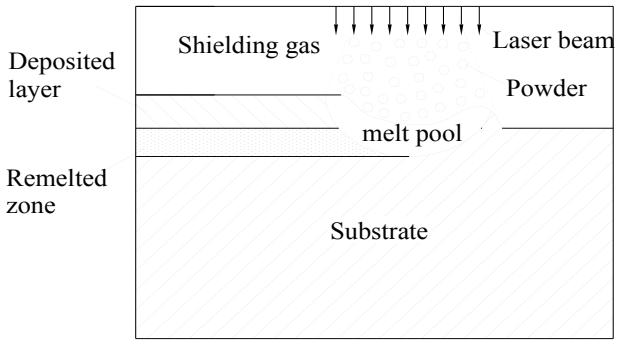


Fig. 2. Schematic of the calculation domain for the macroscopic model

The governing equations have been discretized using a finite volume scheme. The pressure-velocity coupling in the momentum equation is solved using a modified version of the SOLA-VOF algorithm [11]. The thermophysical properties (thermal conductivity, specific heat, etc) are taken as functions of temperature. The material for both metal powder and substrate, Ti-6Al-4V, is taken as a binary alloy. In this way, Ti and Al are considered as a

mixed element X.

Table 1. Summary of the governing equations for the macroscopic model

Continuity

$$\frac{\partial \rho}{\partial t} + \nabla \cdot (\rho \vec{V}) = 0 \tag{10}$$

Momentum

$$\frac{\partial}{\partial t}(\rho \vec{V}) + \nabla \cdot (\rho \vec{V}\vec{V}) = \nabla \cdot (\mu_l \frac{\rho}{\rho_l} \nabla \vec{V}) - \nabla p - \frac{\mu_l}{K} \frac{\rho}{\rho_l} (\vec{V} - \vec{V}_s) + \rho \vec{g} + S_1 \tag{11}$$

$$S_1 = (\vec{n} \gamma \kappa + \nabla_S \gamma) |\nabla F| \frac{F}{\langle F \rangle}$$

(11a)

$$K = \frac{g_l^3}{C(1 - g_l)^2}$$

(11b)

Energy

$$\frac{\partial (\rho h)}{\partial t} + \nabla \cdot (\rho \vec{V} h) = \nabla \cdot (k \nabla T) - \nabla \cdot (\rho (h_l - h)(\vec{V} - \vec{V}_s) + S_2 \tag{12}$$

$$S_2 = \left[ \frac{\eta (P_{laser} - P_{atten})}{\pi R^2} - h_c (T - T_\infty) - \varepsilon \sigma (T^4 - T_\infty^4) - \dot{m}_e L_v \right] |\nabla F| \frac{F}{\langle F \rangle}$$

(12a)

Species

$$\frac{\partial (\rho C)}{\partial t} + \nabla \cdot (\rho \vec{V} C) = \nabla (\rho D \nabla C) + \nabla \left[ \rho D \nabla (C_l - C) \right] - \nabla \left[ \rho (C_l - C)(\vec{V} - \vec{V}_s) \right] \tag{13}$$

Tracking of the free surface

$$\frac{\partial F}{\partial t} + (V \cdot \nabla) F = 0 \tag{14}$$

### 2.3 Coupling between the macroscopic and microscopic models

In the macroscopic model that has been described in the previous section, the temperature field is calculated using finite volume method (FVM) on a fairly coarse grid since the macroscopic model needs to deal with a larger computational domain. The solidification microstructure is simulated on a finer regular Cellular Automaton (CA) mesh. The FVM cells will be re-meshed into CA cells so that the temperature, enthalpy, velocity and solute concentration fields in the macroscopic model are interpolated into the microstructure model. Since the laser deposition process has the nature of rapid solidification and the cooling rates can be very high (as high as 1000-1500 K/s [12]), an adaptive time step is used so that in each time step the peak temperature drop is at the scale of 0.5K. Thus, the temperature, enthalpy, velocity and solute concentration fields are interpolated into the microstructure model both in space and in time. The latent heat release in the microscopic model is interpolated back into the macrostructure model.

## 3. Results and Discussion

In this section, the results of application of the coupled CA model for the evolution of solidification microstructure and the finite volume model for calculation of temperature, fluid flow, solute concentration fields in laser deposition of Ti-6Al-4V are presented and discussed.

Figure 3 shows some macroscopic simulation results: Volume-of-Fluid field and velocity field at t = 20ms, which is used as the starting moment of the microscopic simulation; temperature field at t = 95ms, which is used as the finishing moment of the microscopic simulation. The calculation domain of the microscopic simulation is isolated from the macroscopic calculation domain. At the starting moment of the microscopic simulation, the microscopic domain includes most of the melt pool, part of the gas area, and part of the Heat-Affected-Zone (HAZ). At the finishing moment of the microscopic simulation, the area corresponding to the microscopic domain has been fully solidified. The mesh size for the macroscopic simulation is 20μm and the mesh size for the microscopic simulation is 4μm.

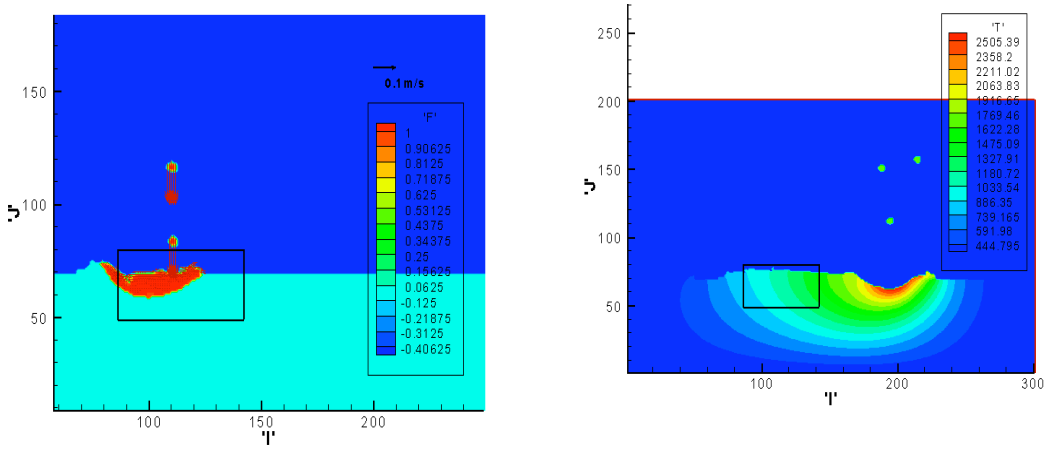


(a) Simulated Volume-of-Fluid field and velocity field from the macroscopic model (t = 20ms)

(b) Simulated temperature field from the macroscopic model (t = 95ms)

Fig.3. Macroscopic simulation results for laser deposition of Ti-6Al-4V using Nd: YAG laser, and isolation of the calculation domain (area delimited by the bold black rectangle) for the microscopic model.

The liquid/solid interface and gas/liquid interface (free surface) are keeping changing during the laser deposition process. From Fig. 4 it can be seen that both of these two types of interfaces are tracked for both macroscopic simulation and microscopic simulation.

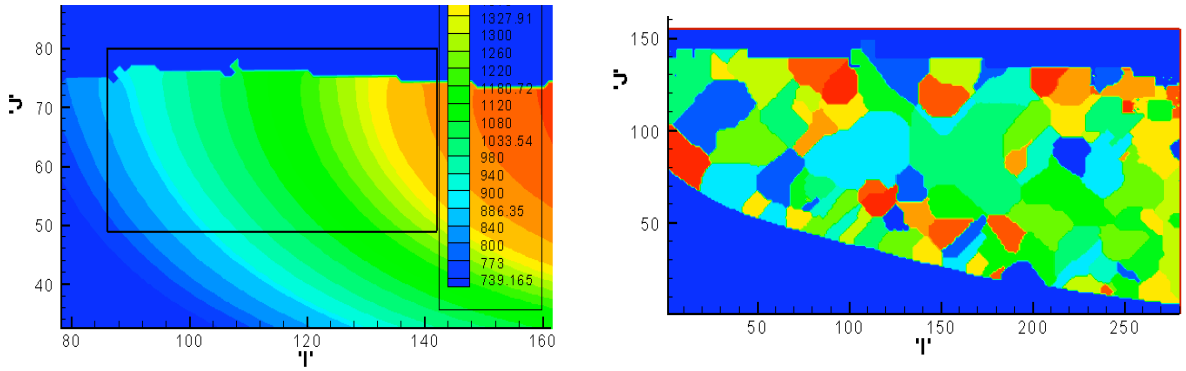


(a) Temperature field of the microscopic calculation domain at t = 95 ms

(b) Simulated solidification microstructure at t = 95 ms

Fig. 4. Macroscopic and microscopic simulation results

Figure 5 shows the evolution of the microstructure during laser deposition. From Fig.5, we can see that grains initially nucleated in the vicinity of the substrate/melt-pool interface and the free surface. This is because that heat extract in these areas is much faster than in the bulk liquid. Also it can be seen that grains nucleated at the substrate/melt-pool interface and the free surface have final small size compared to those nucleated within the bulk liquid. This is because that grains transported into the bulk liquid do not melt and grow the most. So an area of large grains is generally located in the bulk liquid position.

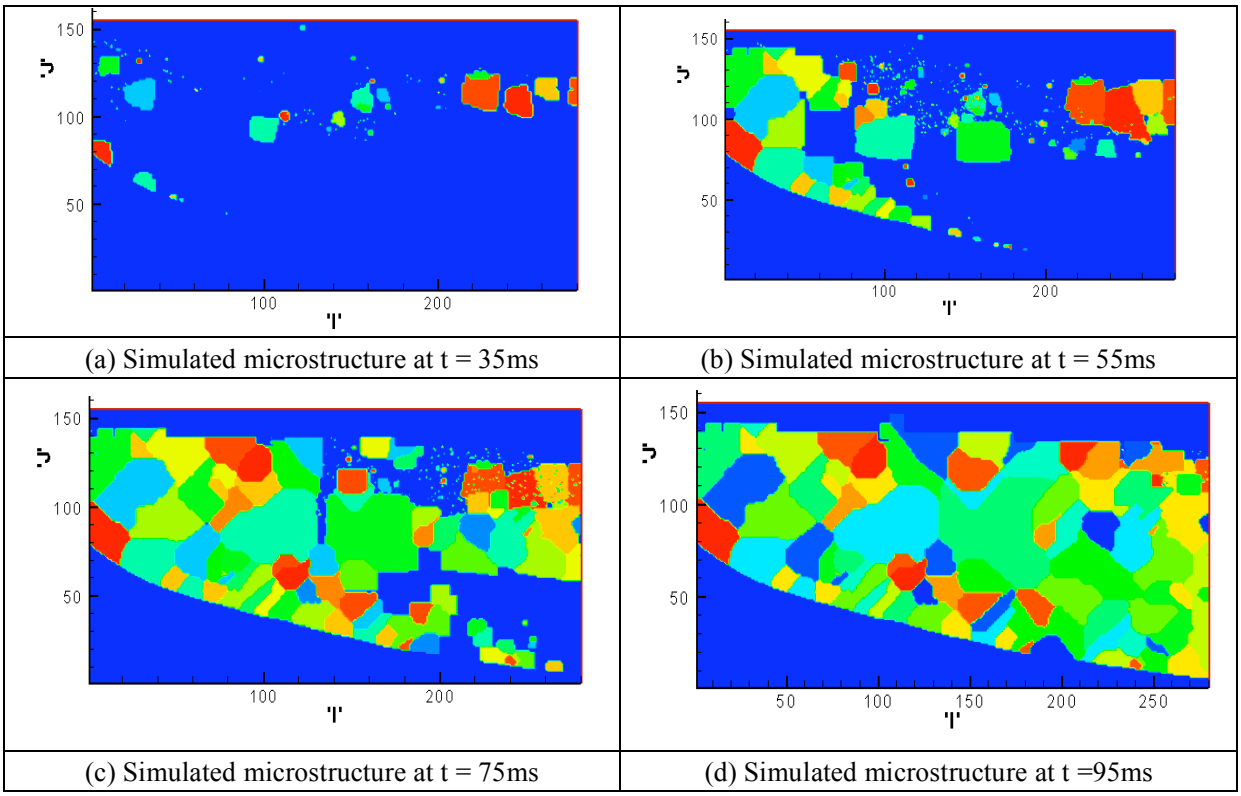


(a) Simulated microstructure at t = 35ms

(b) Simulated microstructure at t = 55ms

(c) Simulated microstructure at t = 75ms

(d) Simulated microstructure at t =95ms

Fig. 5. Simulation of the evolution of the microstructure during laser deposition

The recent simulation results have not yet been compared with the experiments. Before doing so, the following needs to be done. Since the parameters used for the nucleation laws and dendrite growth are critical for the calculation of the grain density and grain size, experiments of laser deposition for the investigated alloy and statistical analysis must be undertaken to determine those parameters.

## 4. Conclusions

The proposed model is able to simulate the evolution of the solidification microstructure during the laser deposition process, including heterogeneous nucleation, dendrite growth, etc. The effect of fluid flow in the melt pool and macrosegregation on the solidification microstructure is accounted for in the current model. The microscopic phenomena during laser deposition are fully coupled with the macroscopic solidification process.


## Acknowledgements

This research was supported by the National Science Foundation Grant Number DMI-9871185, the grant from the U.S. Air Force Research Laboratory contract # FA8650-04-C-5704, and UMR Intelligent Systems Center. Their support is greatly appreciated.


## References:

1. D. Raabe, “Cellular Automata In Materials Science With Particular Reference To Recrystallization Simulation,” Annual Review of Materials Reviews (USA), 2002, Vol. 32, pp. 53-76.
2. G. Guillemot, Ch- A. Gandin, H. Combeau, “Modeling of Macrosegregation and Solidification Grain Structures with a Coupled Cellular Automaton—Finite Element Model,” ISIJ International, Vol. 46 (2006), No. 6, pp. 880–895
3. Ph. Thevoz, J.L. Desbiolles, and M. Rappaz, “Modeling of Equiaxed Microstructure Formation in Casting,” Metall. Trans. A, 1989, vol.20A, pp.311-322.
4. M.J.Aziz, "Nonequilibrium Interface Kinetics During Rapid Solidification: Theory and Experiment", Materials Science and Engineering 98, 369-372 (1988).
5. J. S. Langer and H. Muller-Krumbhaar, “Stability Effects in Dendritic Crystal Growth,” J. Cryst. Growth, 42 (1977), pp. 11-14.
6. W. Kurz, B. Giovanola and R. Trivedi, “Theory of microstructural development during rapid solidification,” Acta Metall., 34 (1986), pp.823-830.
7. Ch.-A. Gandin, G. Guillemot, B. Appolaire and N. T. Niane, “Boundary layer correlation for dendrite tip growth with fluid flow,” Mater. Sci. Eng. A, A342 (2003), pp.44-50.
8. Handbook of Mathematical Functions, Tenth printing, ed. by M. Abramowitz and I. A. Stegun, Dover, USA, 1972.
9. S. Ahuja: Ph. D. Thesis, Iowa University, USA, 1992.
10. Zhiqiang Fan, Master’s thesis, University of Missouri-Rolla, USA, 2007.
11. B. D. Nichols, C.W. Hirt, R. S. Hotchkiss, “SOLA-VOF: A solution algorithm for transient fluid flow with multiple free boundaries,” LA-8355, Los Alamos National Laboratory.
12. Griffith, M. L., Ensz, M. T., Puskar, J. D., Robino, C. V., Brooks, J. A., Philliber, J. A., Smugeresky J. E. and Hofmeister, W. H., “Understanding the microstructure and properties of components fabricated by Laser Engineered Net Shaping (LENS),” Solid Freeform and Additive Fabrication: a Materials Research Society Symposium, San Francisco, CA, USA, 24-26 Apr. 2000. pp. 9-20.